Corrosion Science 51 (2009) 2994–2999

Contents lists available at ScienceDirect

Corrosion Science

journal homepage: www.elsevier.com/locate/corsci

Corrosion study of Alumina/Yttria-Stabilized Zirconia (Al_2O_3/YSZ) nanostructured Thermal Barrier Coatings (TBC) exposed to high temperature treatment

C. Amaya [a,b], W. Aperador [d], J.C. Caicedo [a,*], F.J. Espinoza-Beltrán [c], J. Muñoz-Saldaña [c], G. Zambrano [a], P. Prieto [a]

[a] Department of Physics, Excellence Center for Novel Materials, Universidad del Valle, Cali, Colombia
[b] Hard Coatings Laboratory, CDT-ASTIN SENA, Cali, Colombia
[c] Centro de Investigación y de Estudios Avanzados del IPN, Unidad Querétaro, Mexico
[d] Escuela Ingeniería Mecánica, Escuela Colombiana de Ingeniería, Bogotá, Colombia

ARTICLE INFO

Article history:
Received 12 March 2009
Accepted 11 August 2009
Available online 18 August 2009

Keywords:
Thin films
Thermal Barrier Coatings
Yttria-Stabilized Zirconia
Electrochemical Impedance Spectroscopy

ABSTRACT

Thermal Barrier Coatings (TBC) of 8% Yttria-Stabilized Zirconia (8YSZ) were deposited on AISI-304 substrates via r.f magnetron sputtering. A buffer layer of alumina, Al_2O_3, was deposited to improve the adhesion of the YSZ monolayer to the substrate. The influence of the Al_2O_3/8YSZ coating on the electrochemical conductance evolution, C_t^T, was examined by Electrochemical Impedance Spectroscopy measurements when the steels are exposed to temperatures of 700 and 500 °C for 2, 4, and 6 h. Results indicated that C_t^T diminished three orders of magnitude, in samples coated with Al_2O_3/8YSZ with respect to uncoated steel.

1. Introduction

Micro Air Vehicles (MAV) technology focuses on small flying objects capable of executing useful tasks and those small enough to be operated by one person. MAV typically uses micro gas turbine engines, where alloys, such as austenitic stainless steel and others like nickel-chrome steels are used in the manufacture of blades and turbine discs. These components exhibit, however, a clear decline in terms of strength over time when combustion temperatures reach above 650 °C [1,2] by hot corrosion, which represents a serious limitation in its performance. To improve the thermal efficiency of micro gas turbine engines, increased engine combustion temperature is strongly necessary. In past decades, Thermal Barrier Coating (TBC) systems have been the principal solution to provide protection of metal components, such as turbine blades and nozzles in conditions of high temperature thermal cycling and in corrosive atmospheres [3–6]. A TBC is usually composed of a heat insulating top-coat layer of Yttria-Stabilized Zirconia and a metallic bond-coat layer, used to provide good adhesion, a strong oxidation protection layer for the super alloy substrate [7,41,42]. A variety of techniques has been used to deposit a commercial TBC system, including Air Plasma Spray (APS) [8], Electron Beam-Physical Vapour Deposition (EB-PVD) [9], and *sol–gel* process [10]. However, that Physical Vapour Deposition (PVD) process such as magnetron sputtering, produces TBC coating layers with thicknesses too thin (2–3 μm) relate to the traditional techniques for commercial applications (APS and EB-PVD). At present, these techniques are used in the industry for the production of commercial TBC films for thermal insulating purposes. Such films have thicknesses larger than several tenths of microns. The magnetron sputtering physical vapor deposition technique allows depositing TBC films with thicknesses lower than 3 μm, which show excellent corrosion resistance while maintaining good thermal insulting properties. A significant reduction has been observed in thermal conductivity below 40 nm, due to the fact that thermal conductivity is strongly dependent on grain size; due to nanometer range, phonon scattering increases because the surface-to-volume fraction is enhanced and it provides another mechanism for significantly reducing thermal conductivity with decreasing grain size [11–13]. Additionally, the small spacing between oxygen vacancies and associated small phonon mean-free-path is responsible for the low thermal conductivity of YSZ; moreover a reduction of the film thickness leads to lower mechanical stresses, enhancing the adhesion of films. In addition, thinner films permit less material and time consumption thus reducing the production costs of such industrial coatings. For these nanostructured layers to coat high-performance elements, they must exhibit structural stability when exposed to thermal

* Corresponding author. Tel.: +57 2 339 4610x42; fax: +57 2 339 3237.
E-mail addresses: amayahoy@univalle.edu.co (C. Amaya), wiapch@yahoo.es (W. Aperador), jcesarca@calima.univalle.edu.co (J.C. Caicedo), fespinoza@qro.cinvestav.mx (F.J. Espinoza-Beltrán), jmunoz@qro.cinvestav.mx (J. Muñoz-Saldaña), gzambra@calima.univalle.edu.co (G. Zambrano), pprieto@calima.univalle.edu.co (P. Prieto).

0010-938X/$ - see front matter © 2009 Elsevier Ltd. All rights reserved.
doi:10.1016/j.corsci.2009.08.028

cycles. Among the techniques to assess structural stability in these systems, the Electrochemical Impedance Spectroscopy (EIS), which is a non-destructive technique has helped to establish relations between the electrochemical behaviour, microstructure, and pore evolution of the coating when it is exposed to different temperatures [14], allowing to determinate the damage that the coating can show prior to beginning service [43]. The aim of this study is to address the influence of the Al_2O_3/8YSZ coating on AISI-304 stainless steel upon electrochemical conductance and subsequently exposed to thermal treatment at different temperatures and exposure times, by using the Electrochemical Impedance Spectroscopy (EIS) technique.

2. Experimental procedure

Al_2O_3/8YSZ bilayers were deposited on AISI-304 stainless steel substrates via r.f. (13.56 MHz) magnetron sputtering technique in an Ar (99.99%) atmosphere at a power of 350 W. Zirconia targets of 10 cm diameter doped with 8% mol. Yttria and an Al (99.999%) were used for the preparation of the bilayers. The substrates were cleaned by ultrasound in an acetone/ethanol sequence during 20 min for each cycle. A gradient bond-coat with a compositionally graded structure of Al + Al_2O_3 was deposited onto steel substrates, using high-purity oxygen (99.99%) as working gas. The oxygen flow was systematically increased by using a standard mass-flow controller (MKS 247-D) in steps of 3.5 min for a total time of 20 min. Both, the Al_2O_3 bond-coat and 8YSZ thin films were deposited at constant values of working pressure, temperature, and applied substrate bias voltage of 7.0 μbar, 300 °C and −20 V, respectively. Such conditions were previously found to yield the best adhesion properties of Al_2O_3/8YSZ bilayers to the AISI-304 stainless steel substrate. Isothermal oxidation tests of the obtained Al_2O_3/8YSZ TBC films deposited onto AISI-304 stainless steel were carried out at 500 and 700 °C in air at 2, 4, and 6 h in temperature-control furnace. The electrochemical conductance and corrosion evolution at room temperature of the oxidized samples were characterized by EIS at room temperature in a GAMRY Model PCI 4 flat cell with a volume of 300 ml. For each EIS measurement, the metal side of the oxidized specimen was mechanically polished to remove the oxide layer to avoid potential effects of the EIS measurement (i.e. exposure to electrolyte) on the TBC lifetime. Three electrode system was implemented: the TBC sample, Ag/AgCl, and platinum as working and reference, and counter electrodes, respectively. This system was immersed into a 0.01 M $K_3Fe(CN)_6/K_4Fe(CN)_6$ aqueous solution with a studied surface area of 1 cm^2, and connected to an Echem Analyst EIS measurement system. Nyquist plots were recorded by using a sinusoidal voltage perturbation of 20 mV in a frequency range of 0.001 Hz to 10^5 kHz. Results previously contributed [26] reveal that the advantage of using this electrolyte to measure TBC properties by EIS is based on the fact that at low frequencies, the mass transport behavior of the electrolyte is transformed into a kinetic control step for the electrolyte-filled TBC. Complicated TBC information can be resolved and detailed TBC properties can be extracted from the kinetics of the electrochemical redox reactions as measured by EIS. The electrochemical behaviour of the electrolyte was studied by using EIS at the corrosion potential (E_{corr}) values. The samples were kept in the 0.01 M $K_3Fe(CN)_6/K_4Fe(CN)_6$ aqueous solution for 30 min to establish a stable corrosion potential (E_{corr}) values at which the EIS measurements were initiated, since the experimental EIS parameters, particularly scan rate, will affect both initial and final potential after establishing a stable (E_{corr}). On the other hand, IR compensation was applied by using the interrupted current method and noise reduction was carried out by the GAMRY Model PCI 4 provided software.

3. Results and discussion

Fig. 1(a) and (b) show typical scanning electron microscope (SEM) micrographs of the 8YSZ film cross-sections prepared at −20 V substrate bias voltages. Both the gradient bond-coat of Al_2O_3 and the 8YSZ top-coat layer can be clearly observed with columnar-type growth. The top-coat (Fig. 1b) shows a dense microstructure; probably due to the continual bombardment of the growing film by energetic ions, which serves to increase the surface mobility of adsorbed atoms on the substrate surface, resulting in more compact microstructures. Thus, the prepared Al_2O_3/8YSZ bilayered coatings have nanostructured microstructure and the characteristics are reported elsewhere [15]. The EIS behaviour of the electrolyte, as well as the thermal and non-thermal exposed TBC will be discussed in the next section.

3.1. EIS behaviour of the used electrolyte

The EIS Nyquist plot of the 0.01 M $K_3Fe(CN)_6/K_4Fe(CN)_6$ electrolyte measured at room temperature on a platinum working electrode at the corrosion potential (E_{corr}) values is shown in Fig. 2(a). A schematic of a corresponding a.c. equivalent circuit obtained by simulation from the fitting of the EIS Nyquist plot is also shown in Fig. 2(b), where W is the Warburg impedance, C is the constant phase element, and R_s and R_t^E are the electrolyte resistance

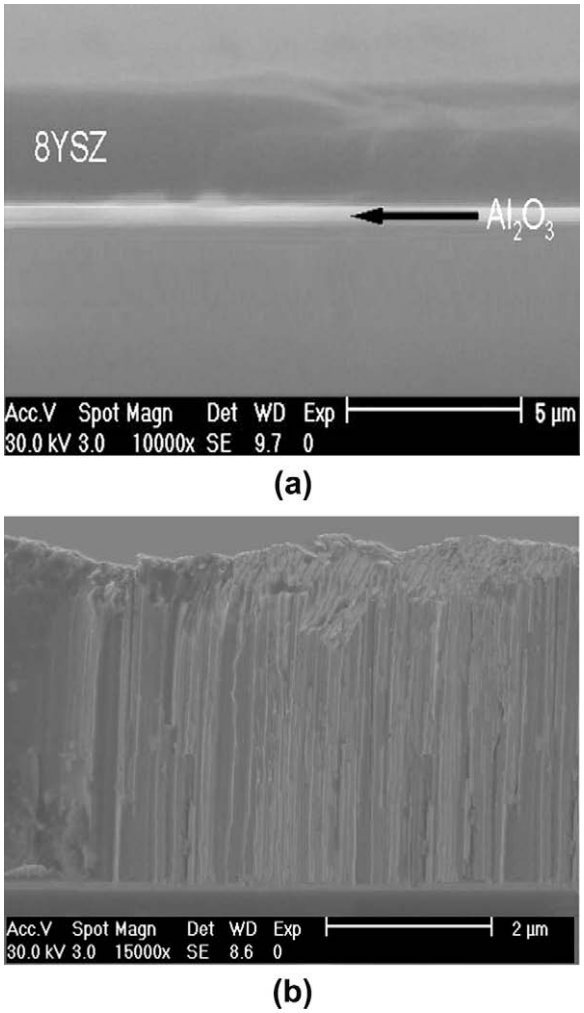

Fig. 1. SEM micrographs of: (a) Al_2O_3/8YSZ bilayered coatings on silicon substrates prepared at −20 V bias voltage, and (b) the microstructure of the 8YSZ top-coat.

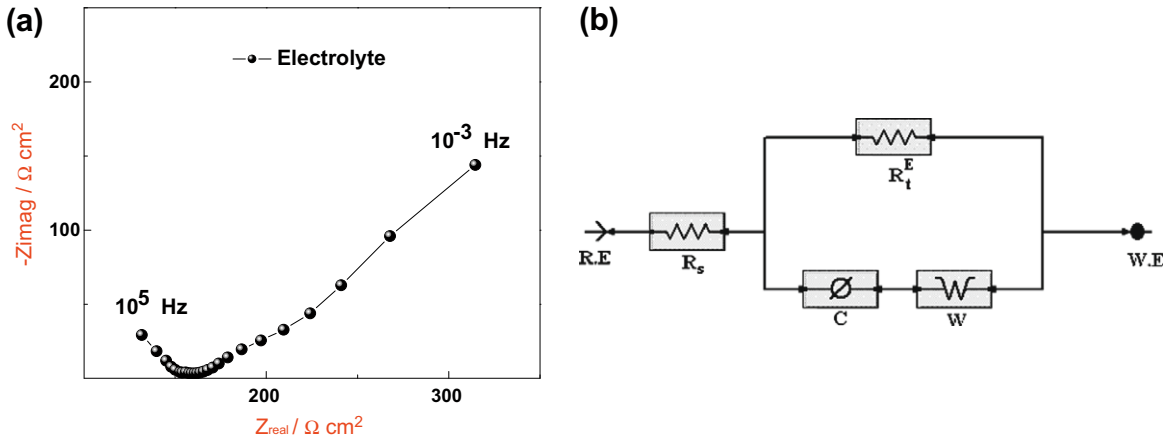

Fig. 2. EIS Nyquist plot of 0.01 M $K_3Fe(CN)_6/K_4Fe(CN)_6$ electrolyte measured on a platinum working electrode (a) and a schematic of corresponding a.c. equivalent circuit (b).

and polarization resistance of the electrolyte, respectively. The numbers given in the Nyquist plot represent the a.c. frequencies corresponding to the measured points. The polarization resistance of the electrolyte, R_t^E $(160.6 \pm 0.2)\,\Omega\,cm^2$ was determined by extrapolating the impedance half-circle to intercept with the real part axis, Z_{real}.

3.2. EIS behaviour of non-thermal exposed TBC

Fig. 3(a) exhibits a typical EIS Nyquist diagram of the AISI-304 without the Al_2O_3/8YSZ bilayer and non-thermal exposed AISI-304/Al_2O_3/8YSZ with 2.5 μm thickness, which clearly consists of a single semi-circle. The equivalent circuit for APS and EB-PVD Thermal Barrier Coatings consists commonly of phase elements of an ideal capacitor, because the YSZ surface roughness, YSZ-bond-coat interfacial roughness, porosity, and pore-shape that give rise to frequency dispersion due to the non-uniform distribution in the current density [16–18]. On the other hand, in a low-dimension system, the thickness of the YSZ top-coat and the bond-coat layer are smaller, and therefore, the pore size and surface roughness have the nanometer scale. Consequently, this nanostructure significantly diminishes the frequency of dispersion in the system. Since the obtained nanostructured TBC deposited by magnetron sputtering method showed a dense structure, free of pores, and the bond-coat consists of a graded structure of Al + Al_2O_3 that allows for a smooth transition on YSZ-bond-coat interface and due to the low thickness of the Al + Al_2O_3 coat layer stack, the a.c. equivalent circuit, Fig. 3(b), that describes our Al_2O_3/8YSZ system can be approximated to a two distributed constant phase elements (C_1 and C_2) to consider the two relaxation time constants. The CPE_1–R_1 couple, which predominates at high frequencies, may be originated by the passivated film and/or the dielectric properties of the interface

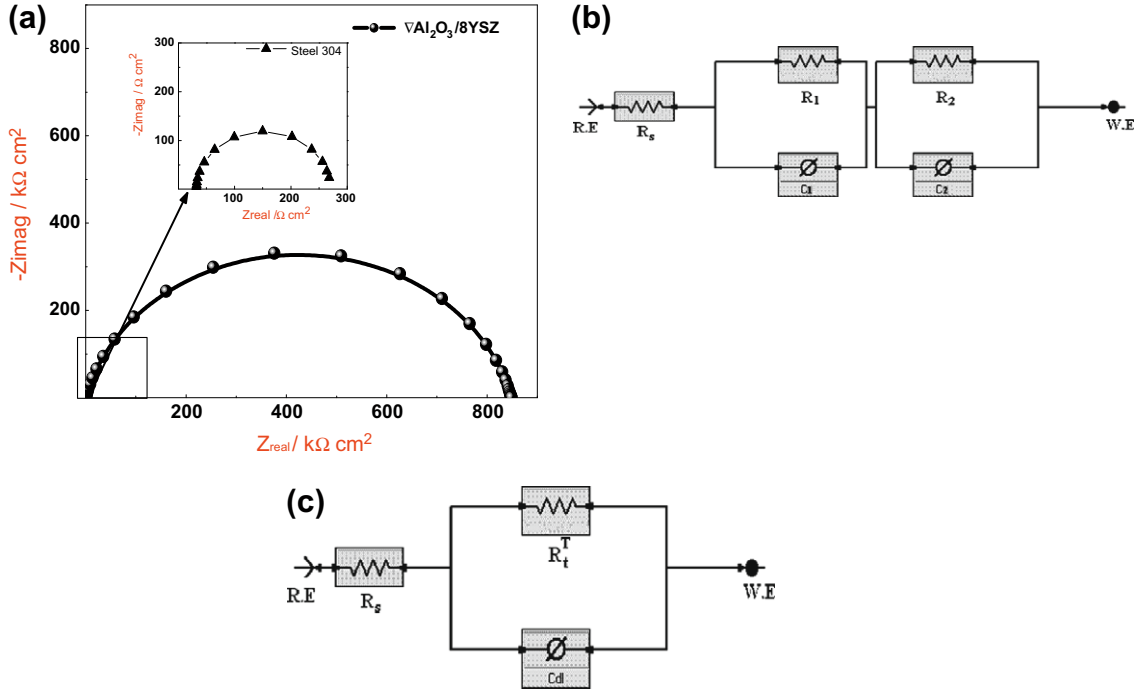

Fig. 3. Schematic of corresponding a.c. equivalent circuit (a) and EIS Nyquist plot of a non-exposed AISI-304 stainless steel without coating and covered with Al_2O_3/8YSZ, measured in an 0.01 M $K_3Fe(CN)_6/K_4Fe(CN)_6$ electrolyte, (b) electrical equivalent circuit used to fit impedance data of Al_2O_3/8YSZ coatings, and (c) electrical equivalent circuit for the Randles cell.

electrolyte/film, while the CPE_2–R_2 couple, controlling at low frequencies, characterizes the corrosion process of the steel/film. On the other hand, the circuit for the Randles cell [19] was used to simulate the obtained interface phenomenon between substrate and coatings, which shows the double layer capacitance that is in parallel with the impedance due to the ion reaction transfer Fig. 3(c) [20,21]. Such an equivalent circuit was previously reported as obtained by simulation from the fitting of the EIS Nyquist plot used in studying the ionic conductivity in YSZ thin films [22] and consists of one resistor and one capacitor in parallel. Further on, the experimental fact of a single semi-circle evidences conditions of good adhesion of prepared Al + Al_2O_3/8YSZ coating systems to the AISI-304 steel [23]. Thus, the polarization resistance, R_t^T of the sample was determined to be $(85.0 \pm 0.1)\,M\Omega\,cm^2$ by extrapolating the impedance half-circle to intercept with the real part axis, Z_{real}. The R_t^T is significantly higher than the polarization resistance of the electrolyte, R_t^E $(160.6 \pm 0.2)\,\Omega\,cm^2$, and of the AISI-304 stainless steel without TBC, R_t^S $(2.7 \pm 0.1) \times 10^2\,\Omega\,cm^2$ as can be noted from Fig. 3(a). The high value obtained for R_t^T can be possibly due to two factors: a dense and homogeneous microstructure that inhibits the inclusion of the electrolyte inside the coating; and the effect of coating thickness. The latter is an effect previously reported by Heung et al. [24]; where it was established that when the thickness of the coating diminishes, the electric field lines are more deviated from vertical electrical field than those in a thick coating and, therefore, the current flow is more restricted. It is well known that TBC coatings deposited by APS and EBPVD techniques are always porous and thick through the whole thickness [41]. However, the very first stages of deposition typically produce a dense microstructure. In the present case, the thickness of the prepared coatings was much smaller (around 2.5 μm) than those reported by Heung. Therefore, it is expected that in our case the value of polarization resistance follows similar behaviour.

3.3. EIS behaviour of thermally exposed TBC

The electrochemical impedance characteristics of TBC depend on the thickness, microstructure, and composition of both the YSZ and the Thermally Grown Oxide (TGO) [22]. Fig. 4(a) and (b) show the EIS Nyquist plots of TBC after exposure to 500 and 700 °C at 2, 4, and 6 h, respectively. The polarization resistance of the TBC is affected by both temperature and time of heat treatment. Particularly, the polarization resistance decreases in all cases with increasing temperature and time of heat treatment. This effect can be associated to the easier penetration of conductive aqueous electrolyte into a porous or microcracked microstructure of the Al_2O_3/8YSZ coating produced after heat treatment. Although the Nyquist plots follow similar behaviour already reported in the literature associated to EB-PVD and APS coatings [25–27]; the present case shows a more dramatic effect again probably due to the micrometric thickness of the coating. Furthermore, it is well known that the substitution of trivalent Y^{3+} cations for the tetravalent Zr^{4+} cation of the host ZrO_2 lattice creates a large concentration of oxygen vacancies by charge compensation, which gives rise to higher oxygen ion mobility [28]. Therefore, YSZ allows some flux of oxygen to diffuse and react with the metallic substrate. The present work incorporated a graded structure of Al + Al_2O_3 because alumina is usually considered the most protective functional graded coating at a broad range of temperatures [29–31,43]. This means that in the YSZ/bond-coat interface an alumina scale was formed, where O^{2-} anions may diffuse inward and/or Al^{3+} cations diffuse outward [32,33] to form a protective alumina layer. The increase of the exposure times and temperature, produces the decrease of the minimum Al content in the bond-coat, required to maintain the Al_2O_3 layer. When this occurs, it is expected to begin to diffuse elements from the metal substrate, which formed other oxides such as iron oxides (FeO) that increase internal tensions, generating high porosity and nucleation of cracks through which the electrolyte penetrates. In addition, these oxides are a fast route for oxygen transport – increasing the ionic conductivity in the circuit, developing, and scaling changes from a process characteristic of a protective regime to one of breakaway oxidation [34,35].

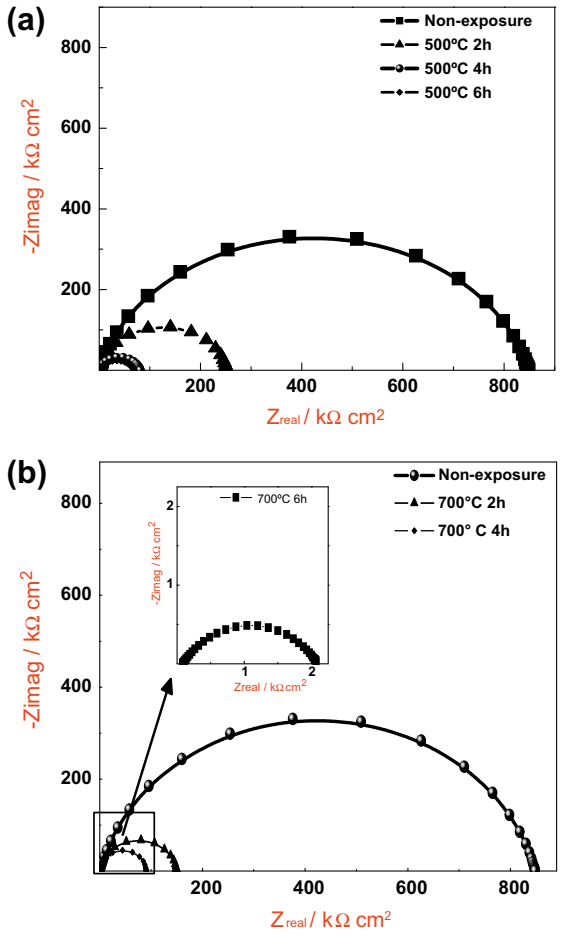

Fig. 4. EIS Nyquist plot of Al_2O_3/8YSZ TBC in the electrolyte after thermal exposure at 500 °C (a) and 700 °C (b) at different exposure times.

3.4. Discussion about the electrochemical conductance evolution

From the Nyquist plots for AISI-304, and Al_2O_3/8YSZ TBC before and after exposure to temperature at different exposure times the polarization resistance, R_t^T, and electrochemical conductance, $C_t^T = \frac{1}{R_t^T}$ were determined. The conductance of AISI-304 steel without TBC was determined as $(3.70 \pm 0.01)\,mS\,cm^{-2}$. A summary of the experimental data of R_t^T and C_t^T for TBC before and after exposure to temperature at different exposure times is presented in Table 1. For the non-exposed Al_2O_3/8YSZ TBC, C_t^T was $(1.18 \pm 0.01)\,\mu S\,cm^{-2}$; while for the exposed TBC at the same temperature but at different exposure times, these values increased one and two orders of magnitude at 500 and 700 °C, respectively. At the same exposure time but at two different temperatures, C_t^T did not change drastically. It is well known that the α-Al_2O_3 phase is the most chemically stable oxide form at 1000 °C, or lower temperatures (approx. 950 °C), but for more prolonged exposure times (<200 h) [35–37]. A highly revealing fact of the prepared TBC systems is the determination of the structural characteristics of the

Table 1
Experimental data of TBC before and after exposure to temperature at different exposure times.

T (°C)	Non-exposure	500			700		
t (h)	0	2	4	6	2	4	6
R_t^T, (±0.1) MΩ cm^2	85.0	25.0	810.0	690.0	15.0	900.0	2100.0
C_t^T, (±0.01) μS cm^{-2}	1.18	3.97	12.30	14.50	6.67	11.10	483.00

TGO. However, such characterization was not the primary goal of the present work and it is not reported here. One would expect that under the present experimental conditions, α-alumina was not formed. Most likely, the formation of mixed oxides of alumina in an amorphous state and iron oxides is expected. Work has to be done to determine the structural and microstructural characteristics of the TGO.

The fact is that with the application of bias voltage and the subsequent surface oxidation of the whole TBC system including the steel substrate, one would expect a decrease of corrosion velocity of the sample. Therefore, at these conditions, C_t^T values are lower than the conductance of AISI-304 without TBC coatings. Again, the Al_2O_3/8YSZ TBC thin films deposited by magnetron sputtering method revealed a dense structure free of pores (Fig. 1) and a similar polarization resistance behaviour compared to that reported by Zhang et al. [26] for 8YSZ coarse coatings deposited by APS, where a linear relationship between thermal conductivity and electrochemical conductance of the YSZ coatings is reported. The use of EIS to evaluate the thermal conductivity of free-standing TBCs is based on the fact that EIS is sensitive to the change in porosity, microstructure transformation and pore evolution of the TBC. Thus, the thermal conductivity is a function of these TBC properties and can be correlated with the EIS parameters [11,26,38–40]. Based on the electrochemical conductance values in Table 1, it is proposed, at least qualitatively, that the Al_2O_3/8YSZ coating still serves as an ionic and thermal barrier of the metal substrate [42,43]. The use of the Zhang et al. model to adjust the behaviour of TBC's thin films prepared by r.f. magnetron sputtering remain s open for future studies; where EIS can be used as a non-destructive technique to access and monitor the thermal conductivity values in thin films.

4. Conclusions

Thin films of Al_2O_3/8YSZ were deposited onto AISI-304 stainless steel substrates by r.f. multi-target magnetron sputtering and indirectly evaluated as a TBC by measuring their electrochemical behaviour at different temperatures and exposure times. The applied substrate bias voltage during deposition process of 8YSZ TBC allowed obtaining a dense structure of the thin films, resulting in an increase of polarization resistance and a decrease of conductance of AISI-304/Al_2O_3/8YSZ by three orders of magnitude with respect to the steel without TBC. After exposure time at different temperatures of the AISI-304/Al_2O_3/8YSZ stack, the reduction in polarization resistance and the increase of the conductance should be ascribed to pore evolution and microstructure transformation in the TBC with sintering. However, at a higher temperature (700 °C) and exposure time (6 h), polarization resistance is higher and conductance is one order of magnitude lower with respect to this parameter of AISI-304 steel without TBC and not exposed to temperature. The change in polarization resistance is ideally compatible with the change in thermal conductivity of the TBC just as reported by Zhang et al. Therefore, we can conclude that the present experimental conditions lead to AISI-304/Al_2O_3/8YSZ film structure with indirectly determined lower thermal conductivity compared to the metallic substrate. Hence, the Al_2O_3/8YSZ deposited film system opens the possibility of increasing the performance of micro gas turbine metallic elements exposed to elevated operation temperatures.

Acknowledgements

This work was supported by the Center of Excellence for Novel Materials (CENM) under Colciencias/CENM contract # RC-043-2005. Colciencias-Univalle.

References

[1] Thomas Kamps, Keith Thomas, Model Jet Engines, third ed., Traplet Publications, New York, 2005. p. 70.
[2] G. Scheffknecht, Q. Chen, G. Weissinger, in: A. Strang, (Ed.), Proceedings of the Sixth International Charles Parsons Turbine Conference, Maney, London, 2003, p. 113.
[3] Lech Pawlowski, The Science and Engineering of Thermal Spray Coatings, John Wiley & Sons, New York, 1995. p. 314.
[4] Douglas E. Wolfe, Jogender Singh, Robert A. Miller, Jeff I. Eldrigdge, Dong-Ming Zhu, Surf. Coat. Technol. 190 (2005) 132.
[5] X.Q. Cao, R. Vassen, D. Stoever, J. Eur. Ceram. Soc. 24 (2004) 1.
[6] G.W. Goward, Surf. Coat. Technol. 108 (1998) 73.
[7] Z. Yu, D.D. Hass, H.N.G. Wadley, Mater. Sci. Eng. A 394 (2005) 43.
[8] P. Scardi, L. Lutterotti, Surf. Coat. Technol. 61 (1993) 52.
[9] D.D. Hass, A.J. Slifka, H.N.G. Wadley, Acta Mater. 49 (2001) 973.
[10] A. Meher, H. Klumper-Westkamp, F. Hoffmann, P. Mayr, Thin Solid Films 308 (1997) 673.
[11] G. Soyez, J.A. Eastman, L.J. Thompson, G.R. Bai, P.M. Baldo, A.W. McCormick, R.J. DiMelfi, A.A. Elmustafa, M.F. Tambwe, D.S. Stone, Appl. Phys. Lett. 77 (8) (2000) 1155.
[12] Ho-Soon Yang, G.-R. Bai, L.J. Thompson, J.A. Eastman, Acta Mater. 50 (2002) 2309.
[13] David G. Cahill, Wayne K. Ford, Kenneth E. Goodson, Gerald D. Mahan, Arun Majumdar, Humprey J. Maris, Roberto Merlin, Simon R. Phillpot, J. Appl. Phys. 93 (2003) 2.
[14] S.-H. Song, P. Xiao, L.-Q. Weng, J. Eur. Ceram. Soc. 25 (2005) 1167.
[15] C. Amaya, J.C. Caicedo, G. Bejarano, C.A. Cortés Escobedo, J. Muñoz-Saldaña, G. Zambrano, P. Prieto, Phys. Status Solidi (c) 4 (11) (2007) 4288.
[16] B. Jayaraj, V.H. Desai, C.K. Lee, Y.H. Sohn, Mat. Sci. Eng. A. 372 (2004) 278–286.
[17] A. Conde, J.J. de Damborenea, Corros. Sci. 44 (2002) 1555.
[18] R. de Levie, Electrochim. Acta 10 (1965) 395.
[19] J.E.B. Randles, Discuss. Faraday Soc. 1 (1947) 11–18.
[20] D.V. Shtansky, Multicomponent nanostructured thin films, in: A.A. Voevodin, D.V. Shtansky, E.A. Levashov, J.J. Moore (Eds.), Deposition, Characterization, Testing and Application. Nanostructured Thin Films and Nanodispersion Strengthened Coatings, NATO Series, Kluwert Academic Publishers, 2004. pp. 155–166.
[21] S. Surviliene, S. Bellozor, M. Kurtinaitiene, V.A. Safonov, Surf. Coat. Technol. 176 (2004) 193–201.
[22] E.B. Ramírez, A. Huanosta, J.P. Sebastián, L. Huerta, A. Ortiz, J.C. Alonso, J. Mater. Sci. 42 (3) (2007) 901.
[23] Luis E.M. Palomino, Patricia H. Suegama, Idalina V. Aoki, Zoltán Pászti, Hercílio G. de Melo, Electrochim. Acta 52 (2006) 7496.
[24] R. Heung, X. Wang, P. Xiao, Electrochim. Acta 51 (2006) 1789.
[25] B. Jayaraj, S. Vishweswaraiah, V.H. Desai, Y.H. Sohn, Surf. Coat. Technol. 177 (2004) 140.
[26] J. Zhang, V. Desai, Surf. Coat. Technol. 190 (2005) 90.
[27] Md. Shawkat Ali, Shenhua Song, Ping Xiao, J. Eur. Ceram. Soc. 22 (2002) 101.
[28] N.Q. Minh, J. Am. Ceram. Soc. 76 (1993) 563.
[29] B.A. Pint, J.R. DiStefano, I.G. Wright, Mater. Sci. Eng. A 415 (2006) 255.
[30] Huibin Xu, Hongbo Guo, Fushun Liu, Shengkai Gong, Surf. Coat. Technol. 130 (2000) 133.
[31] B.A. Movchan, G.S. Marinski, Surf. Coat. Technol. 100 (1998) 309.
[32] J.S. Sheasby, D.B. Jory, Oxid. Met. 12 (1977) 527.
[33] D. Nicolas-Chaubet, A.M. Huntz, F. Millot, J. Mater. Sci. 26 (22) (1991) 6113.
[34] P.F. Tortorelli, U.K. Natesan, Mater. Sci. Eng. A 258 (1998) 115.
[35] K. Natesan, Mater. Sci. Eng. A 258 (1998) 126.
[36] P.F. Tortorelli, J.H. DeVan, Mater. Sci. Eng. A 153 (1992) 573.
[37] Shenhua Song, Ping Xiao, Mater. Sci. Eng. B 97 (2003) 46.
[38] P.G. Klemens, M. Gell, Mater. Sci. Eng. A 245 (1998) 143.
[39] U. Schulz, J. Am. Ceram. Soc. 83 (4) (2000) 904.

[40] Paolo Scardi, Matteo Leoni, Federico Cernuschi, Angelamaria Figari, J. Am. Ceram. Soc. 84 (4) (2001) 827.
[41] Z.F. Zhou, E. Chalkova, S.N. Lvov, P. Chou, R. Pathania, Corros. Sci. 49 (2) (2007) 830–843.
[42] R. Podor, N. David, C. Rapin, M. Vilasi, P. Berthod, Corros. Sci. 49 (8) (2007) 3226–3240.
[43] L.M. Palomino, P.H. Suegama, I.V. Aoki, M.F. Montemor, H.G. De Melo, Corros. Sci. 51 (6) (2009) 1238–1250.